# Finite Element Waveguide Solvers Revisited

Ortwin FARLE, Volker HILL, and Romanus DYCZIJ-EDLINGER, *Member, IEEE*

***Abstract*— A general analysis of potential- or field-based finite element solvers for axially uniform electromagnetic waveguides is presented. Explicit equations for the set of permissible gauge transformations are derived, which are later utilized to identify side effects that may affect the reliability of present approaches. We show that such limitations can be eliminated by an enhanced formulation employing a decomposition of the transverse components of the vector potential together with a particular choice of gauge. Numerical results support our findings.**

***Index Terms*— Electromagnetic fields, finite element methods, eigenvalue problems.**

## I. Introduction

ELECTROMAGNETIC waveguides are often characterized by inhomogeneous material properties and/or complicated shapes. Since analytical solutions for the modal field patterns or propagation characteristics of such structures are usually not available, efficient numerical methods [1] [2] [3] are of great practical importance.

Thanks to its great flexibility in geometry and material approximation, the finite element (FE) method is particularly well-suited for waveguide analysis. Early node-based FE implementations struggled with the occurrence of spurious modes [2], but with the advent of $H(curl)$ elements [4] [5], the reliability of such methods vastly improved [6]-[8]. Even though the scope of today's FE codes ranges from anisotropic materials [7] [8] [9] to reduced order modelling [10] [11], almost any full-wave solver fits into one of two major categories of formulations.

The first type employs a system of two coupled first order partial differential equations (PDEs). Even though these methods boast a number of very appealing features, e.g. comparable accuracy for both electric and magnetic fields, they are outside the scope of this paper.

Second, there are methods that directly implement the time-harmonic form of the vector wave equation. Specific formulations may employ fields [6]-[8] or potentials [9] [10] and, in the latter case, they may differ in their choice of gauge. Even though all variants perform well in the majority of applications, there are certain situations, e.g. close to cut-off or in the low-frequency case, where specific implementations may prove disadvantageous. The present article develops a common framework for the whole family of formulations, which is then used to analyze the characteristics of typical implementations. Based on our findings, we propose an improved formalism which eliminates side effects that may affect the reliability of present approaches.

Manuscript received July 1, 2003.

The authors are with Lehrstuhl für Theoretische Elektrotechnik, Dept. of Electrical Engineering, Saarland University, Saarbrücken, D-66123, Germany (telephone (+49) (+681) 302-2441, e-mail: roman.edlinger@ieee.org).

## II. Potential Formulation

Assuming a source-free region and scalar-valued, lossless material properties, the time-harmonic form of the Maxwell equations is given by

$$\nabla \times \vec{H} = jk_0/\eta_0 \epsilon_r \vec{E}, \tag{1}$$

$$\nabla \times \vec{E} = -jk_0 \eta_0 \mu_r \vec{H}, \tag{2}$$

$$\nabla \cdot \vec{B} = 0, \tag{3}$$

$$\nabla \cdot \vec{D} = 0, \tag{4}$$

where $k_0$, $\eta_0$, and $c_0$ denote the free space wavenumber, characteristic impedance, and speed of light, respectively. In terms of a magnetic vector potential $\vec{A}$ and an electric scalar potential $\phi$, we obtain the equations

$$\vec{B} = \nabla \times \vec{A}, \tag{5}$$

$$\vec{E} = -c_0 \nabla \phi - jk_0 c_0 \vec{A}, \tag{6}$$

$$0 = \nabla \times \mu_r^{-1} \nabla \times \vec{A} - k_0 \epsilon_r (k_0 \vec{A} - j\nabla\phi), \tag{7}$$

$$0 = \nabla \cdot \epsilon_r (k_0 \vec{A} - j\nabla\phi). \tag{8}$$

Note that we have stated (8) because in the static limit, $k_0 \to 0$, (7) does not impose (4) anymore. Thanks to uniformity along the waveguide axis $z$, we may write

$$\nabla = \nabla_t - \gamma \hat{e}_z, \tag{9}$$

$$\vec{A} = e^{-\gamma z} \left( \vec{A}_t(x,y) + A_z(x,y)\hat{e}_z \right), \tag{10}$$

$$\phi = e^{-\gamma z} V(x,y), \tag{11}$$

where $\gamma$ stands for the propagation constant, subscript $t$ for transversal components, and $\hat{e}_z$ for the unit vector in axial direction. Now the key point for our analysis is to split $\vec{A}_t$ into a transverse gradient $\nabla_t \psi$ plus a function $\vec{A}_t^c$ of non-vanishing circulation,

$$\vec{A}_t(x,y) = \vec{A}_t^c(x,y) + \nabla_t \psi(x,y). \tag{12}$$

By plugging (9) - (12) into (5) - (8), we arrive at

$$\vec{B} = e^{-\gamma z} \{ \nabla_t \times \vec{A}_t^c - \hat{e}_z \times [\gamma \vec{A}_t^c + \nabla_t(\gamma\psi + A_z)] \}, \tag{13}$$

$$\begin{aligned} \vec{E} = e^{-\gamma z} \{ & -jc_0 [k_0 \vec{A}_t^c + \nabla_t (k_0 \psi - jV)] \\ & - jc_0 [k_0(\gamma\psi + A_z) - \gamma(k_0\psi - jV)]\hat{e}_z \}. \end{aligned} \tag{14}$$

$$\begin{aligned} 0 = {} & \nabla_t \times \mu_r^{-1} \nabla_t \times \vec{A}_t^c + \gamma^2 \hat{e}_z \times \mu_r^{-1} \hat{e}_z \times \vec{A}_t^c - k_0^2 \varepsilon_r \vec{A}_t^c \\ & + \gamma \hat{e}_z \times \mu_r^{-1} \hat{e}_z \times \nabla_t (\gamma\psi + A_z) \\ & - k_0 \varepsilon_r \nabla_t (k_0 \psi - jV), \end{aligned} \tag{15}$$

$$\begin{aligned} 0 = {} & -\gamma \hat{e}_z \cdot (\nabla_t \times \mu_r^{-1} \hat{e}_z \times \vec{A}_t^c) \\ & - \hat{e}_z \cdot (\nabla_t \times \mu_r^{-1} \hat{e}_z \times \nabla_t (\gamma\psi + A_z)) \\ & - k_0^2 \varepsilon_r (\gamma\psi + A_z) + \gamma k_0 \varepsilon_r (k_0 \psi - jV). \end{aligned} \tag{16}$$

$$\begin{aligned} 0 = {} & \nabla_t \cdot \epsilon_r [k_0 \vec{A}_t^c + \nabla_t (k_0 \psi - jV)] \\ & + \gamma \epsilon_r [\gamma(k_0\psi - jV) - k_0(\gamma\psi + A_z)]. \end{aligned} \tag{17}$$

Eqs. (15)-(17) provide a common basis for a broad variety of waveguide solvers. Specific implementations differ mainly in the choice of gauge.

## III. Permissible Gauge Transformations

Since the formulation (15)-(17) contains three different types of scalar functions, we ought to clarify what constraints one may impose on the system without affecting the generality of the field approximation. Eqs. (13) and (14) show that the EM fields just depend on two independent linear combinations of $V$, $\psi$, and $A_z$ rather than all three scalars. By substituting

$$\alpha(x,y) = \gamma\ \psi(x,y) + A_z(x,y), \tag{18}$$
$$\beta(x,y) = k_0\psi(x,y) - jV(x,y) \tag{19}$$

for the relevant terms, we obtain

$$\vec{B}(x,y) = \nabla_t \times \vec{A}_t^c - \hat{e}_z \times (\gamma\vec{A}_t^c + \nabla_t\alpha), \tag{20}$$
$$\vec{E}(x,y) = -jc_0(k_0\vec{A}_t^c + \nabla_t\beta) - jc_0(k_0\alpha - \gamma\beta)\hat{e}_z. \tag{21}$$

Eqs. (20) and (21) imply that, to avoid non-physical restrictions on the electromagnetic fields, the gauge must not impose any constraints on the scalar functions $\alpha(x,y)$ and $\beta(x,y)$.

To analyze the effects of specific gauges, we must first clarify the details of our computer implementation.

## IV. Finite Element Representation

In case of lowest order elements, we represent $\vec{A}_t^c$ by the co-tree variables of edge elements [12] and the scalar-valued functions $A_z$, $\psi$, and $V$ by the corresponding nodal basis. In case of multiple non-connected perfect electric conductors (PEC), we choose a forest rather than a tree and set

$$\vec{A}_t^c = 0, \qquad A_z = V = \psi = 0 \qquad \text{on PECs.} \tag{22}$$

By applying Galerkin's method to (15)-(17), we arrive at a algebraic quadratic eigenvalue problem (QEP) of the form

$$\left( \begin{bmatrix} S_{AA}^{\nu} - k_0^2 T_{AA}^{\varepsilon} & -k_0^2 C_{AV}^{\varepsilon} & 0 & k_0 C_{AV}^{\varepsilon} \\ -k_0^2 C_{AV}^{\varepsilon T} & -k_0^2 S_{VV}^{\varepsilon} & 0 & k_0 S_{VV}^{\varepsilon} \\ 0 & 0 & k_0^2 T_{VV}^{\varepsilon} - S_{VV}^{\nu\times} & 0 \\ k_0 C_{AV}^{\varepsilon T} & k_0 S_{VV}^{\varepsilon T} & 0 & -S_{VV}^{\varepsilon} \end{bmatrix} \right.$$
$$- \gamma \begin{bmatrix} 0 & 0 & B_{AV}^{\nu\times} & 0 \\ 0 & 0 & S_{VV}^{\nu\times} & 0 \\ B_{AV}^{\nu\times T} & S_{VV}^{\nu\times T} & 0 & -k_0 T_{VV}^{\varepsilon} \\ 0 & 0 & -k_0 T_{VV}^{\varepsilon T} & 0 \end{bmatrix}$$
$$\left. - \gamma^2 \begin{bmatrix} T_{AA}^{\nu\times} & B_{AV}^{\nu\times} & 0 & 0 \\ B_{AV}^{\nu\times T} & S_{VV}^{\nu\times} & 0 & 0 \\ 0 & 0 & 0 & 0 \\ 0 & 0 & 0 & -T_{VV}^{\varepsilon} \end{bmatrix} \right) \begin{bmatrix} \mathbf{v}_{A_t^c} \\ \mathbf{v}_{\psi} \\ \mathbf{v}_{A_z} \\ \mathbf{v}_{jV} \end{bmatrix} = \begin{bmatrix} 0 \\ 0 \\ 0 \\ 0 \end{bmatrix}, \tag{23}$$

where $\mathbf{v}$ stands for an unknown coefficient vector. By denoting $H^1$ and $H(curl)$ basis functions by $W$ and $\vec{w}$, respectively, the sub-matrices of (23) take the form

$$[S_{AA}^{\nu}]_{ik} = \int \nabla_t \times \vec{w}_i \cdot \nu_r \nabla_t \times \vec{w}_k\, d\Omega, \tag{24}$$
$$[T_{AA}^{\varepsilon}]_{ik} = \int \vec{w}_i \cdot \varepsilon_r \vec{w}_k\, d\Omega, \tag{25}$$
$$[C_{AV}^{\varepsilon}]_{ik} = \int \vec{w}_i \cdot \varepsilon_r \nabla_t W_k\, d\Omega, \tag{26}$$
$$[S_{VV}^{\varepsilon}]_{ik} = \int \nabla_t W_i \cdot \varepsilon_r \nabla_t W_k\, d\Omega, \tag{27}$$
$$[S_{VV}^{\nu\times}]_{ik} = \int (\hat{e}_z \times \nabla_t W_i) \cdot (\nu_r \hat{e}_z \times \nabla_t W_k)\, d\Omega, \tag{28}$$
$$[B_{AV}^{\nu\times}]_{ik} = \int (\hat{e}_z \times \vec{w}_i) \cdot (\nu_r \hat{e}_z \times \nabla_t W_k)\, d\Omega, \tag{29}$$
$$[T_{AA}^{\nu\times}]_{ik} = \int (\hat{e}_z \times \vec{w}_i) \cdot (\nu_r \hat{e}_z \times \vec{w}_k)\, d\Omega, \tag{30}$$
$$[T_{VV}^{\varepsilon}]_{ik} = \int W_i \varepsilon_r W_k\, d\Omega. \tag{31}$$

## V. Shift-and-Invert Arnoldi Solver

Since only a few eigenfunctions of certain spectral properties are of interest, e.g. the lowest order modes, a method that finds eigenvalues selectively is employed. As will be detailed below, we transform (23) to an ordinary linear eigenvalue problem, which we solve by the public domain ARPACK solver in shift-and-invert mode. Given a guess $\bar{\lambda}$ for the eigenvalue of the sought mode, we have

$$A\mathbf{v} = \lambda B\mathbf{v}, \tag{32}$$
$$\epsilon := \lambda - \bar{\lambda}, \qquad |\epsilon| \ll |\lambda|, \tag{33}$$
$$(A - \bar{\lambda}B)^{-1}B\mathbf{v} = \frac{1}{\epsilon}\mathbf{v}. \tag{34}$$

## VI. Non-physical Modes and Orthogonalization

As we will show in Sections VII - IX, formulations based on (15)-(17) all support large sets of non-physical modes. However, their field patterns $\mathbf{v}$ are explicitly known and, depending on the gauge, the corresponding eigenvalues are all zero or at infinity. Still, the presence of non-physical null-eigenvalues may affect the reliability of the eigenvalue solver. Depending on the quality of the shift $\bar{\lambda}$, the eigensolver may return physical or non-physical solutions. In the vicinity of cut-off of a physical mode, the situation gets even worse. Since its propagation constant approaches zero, physical and non-physical mode patterns may mix, which strongly deteriorates numerical convergence. To overcome this problem, we utilize the generalized orthogonality relation

$$\mathbf{v}_i^T B\mathbf{v}_k = 0 \qquad \text{for } i \neq k, \tag{35}$$

to orthogonalize both initial vector and iterated residuals with respect to all non-physical null-eigenvectors.

## VII. V-Gauge and Field Formulation

Let us impose the gauge by setting $V \equiv 0$. We now have

$$\beta(x,y) = k_0\psi(x,y). \tag{36}$$

Since $k_0 \to 0$ enforces $\beta \to 0$, the scalar function $\beta(x,y)$ fails to serve as an independent variable in the static limit, causing numerical instabilities in the low frequency case. In practice, one prefers the linearized [6] eigenvalue problem (23), which is obtained by setting $A_z = \gamma\tilde{A}_z$ and multiplying (16) by $\gamma$. To reveal the details of the failure mechanism, consider the subspace $\vec{A}_t^c = 0$. Eqs. (15) (16) now yield

$$0 = -k_0^2\varepsilon_r\nabla_t\psi + \gamma^2\hat{e}_z \times \mu_r^{-1}\hat{e}_z \times \nabla_t(\psi + \tilde{A}_z) \tag{37}$$
$$0 = \gamma^2\nabla_t \times \mu_r^{-1}\hat{e}_z \times \nabla_t(\psi + \tilde{A}_z) - \gamma^2 k_0^2\varepsilon_r\tilde{A}_z\hat{e}_z. \tag{38}$$

and, for $k_0 \to 0$, they become linearly dependent,

$$0 = \gamma^2\hat{e}_z \times \mu_r^{-1}\hat{e}_z \times \nabla_t(\psi + \tilde{A}_z), \tag{39}$$
$$0 = \gamma^2\nabla_t \times \mu_r^{-1}\hat{e}_z \times \nabla_t(\psi + \tilde{A}_z). \tag{40}$$

Hence the matrices $A$ and $B$ in (34) both become singular and share a common nullspace, whose dimension equals the

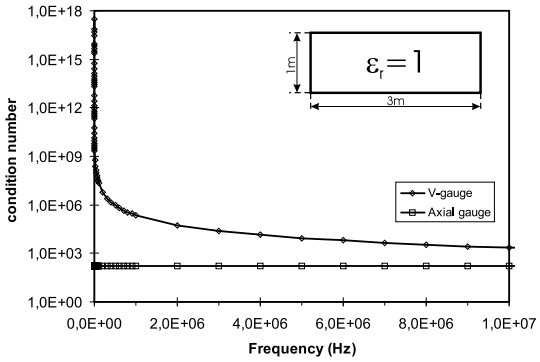


Fig. 1. Rectangular waveguide: Condition number of matrix $(A - \bar{\lambda}B)^{-1}$ for $\bar{\lambda} = 1.0$.

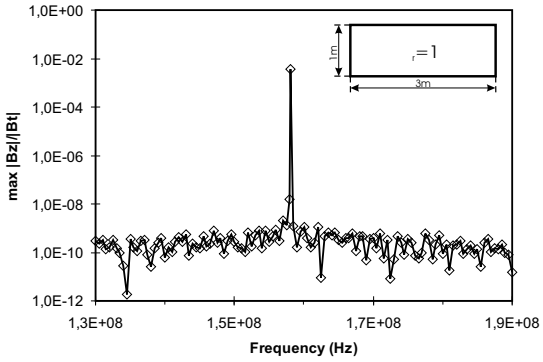


Fig. 2. Maximum of ratio $|B_z|/|\vec{B}_t|$ for $TM_{11}$ mode.

number of free nodes $N$. As a result, the matrix $(A - \bar{\lambda}B)^{-1}$ becomes highly singular no matter what shift is chosen, and the shift-and-invert strategy breaks down. Fig. 1 shows the condition number of this matrix as a function of frequency.

Eq. (6) shows that the field formulation is equivalent to the present method but for a scaling factor of $-jc_0k_0$. Hence field-based algorithms [6] [13] [7] are expected to exhibit the same behavior as the V-gauge approach. Also, notice the occurrence of wave-number independent null field solutions [6],

$$\gamma = 0; \quad \tilde{A}_z \text{ arbitrary}, \psi = 0, \vec{A}_t^c = 0; \quad \vec{B} = 0, \vec{E} = 0. \quad (41)$$

As explained in Section VI, methods without orthogonalization [6] [13] [7] may have trouble identifying a physical mode at wavenumbers in the close vicinity of cut-off. In view of (35), we suggest to explicitly enforce

$$\mathbf{v}_\psi = -S_{VV}^{\nu\times T-1}[B_{AV}^{\nu\times T}\mathbf{v}_{A_t^c} + (S_{VV}^{\nu\times} - k_0^2 T_{VV}^{\varepsilon})\mathbf{v}_{A_z}]. \quad (42)$$

## VIII. Axial Gauge

Choosing $A_z(x, y) \equiv 0$ [9] for the gauge is very appealing, because it reduces (23) to a linear eigenvalue problem for $\gamma^2$. There are no problems in the static limit, see Fig. 1 for the condition number of $(A - \bar{\lambda}B)^{-1}$, but we now get wavenumber-independent null-field solutions [10] of the form

$$\gamma = 0; \ \psi \text{ arbitrary}, jV = k_0\psi, \vec{A}_t^c = 0; \ \vec{B} = 0, \vec{E} = 0, \quad (43)$$

$$\mathbf{n} = \begin{bmatrix} 0 & I & k_0 I \end{bmatrix}^T \mathbf{n}_\psi \qquad \mathbf{n}_\psi \text{ arbitrary}, \quad (44)$$

where $\mathbf{n}$ denotes the corresponding coefficient vector. To suppress null-field solutions and avoid problems with physical modes close to cut-off, we apply (35). By plugging (44) and the rightmost matrix from (23) into (35), we arrive at

$$\mathbf{n}_\psi^T \begin{bmatrix} 0 & I & k_0 I \end{bmatrix} \begin{bmatrix} T_{AA}^{\nu\times} & B_{AV}^{\nu\times} & 0 \\ B_{AV}^{\nu\times T} & S_{VV}^{\nu\times} & 0 \\ 0 & 0 & -T_{VV}^{\varepsilon} \end{bmatrix} \begin{bmatrix} \mathbf{v}_{A_t^c} \\ \mathbf{v}_\psi \\ \mathbf{v}_{jV} \end{bmatrix} = 0, \quad (45)$$

$$\mathbf{v}_\psi = S_{VV}^{\nu\times -1}(k_0 T_{VV}^{\varepsilon}\mathbf{v}_{jV} - B_{AV}^{\nu\times T}\mathbf{v}_{A_t^c}). \quad (46)$$

Eq. (46) underlines the importance of splitting $\vec{A}_t$ as in (12). In the older approach without $\psi$ [10], orthogonality can only be imposed by

$$\mathbf{v}_{jV} = \frac{1}{k_0} T_{VV}^{\varepsilon -1} B_{AV}^{\nu\times T}\mathbf{v}_{A_t}, \quad (47)$$

which clearly breaks down in the static limit.

One issue with the axial gauge is that $\alpha = \gamma\psi$. At $\gamma = 0$, we have

$$\alpha(x, y) = 0, \quad (48)$$

$$\vec{B}(x, y) = \nabla_t \times \vec{A}_t^c \qquad \| \hat{e}_z, \quad (49)$$

$$\vec{E}(x, y) = -jc_0(k_0\vec{A}_t^c + \nabla_t\beta) \qquad \perp \hat{e}_z. \quad (50)$$

For (49) and (50) imply $\vec{B} \parallel \hat{e}_z$ and $\vec{E} \perp \hat{e}_z$, one might expect serious cancellation when recovering the fields of transverse magnetic (TM) modes close to cut-off from the potential solutions. To measure such cancellation, we considered the $TM_{11}$ mode of a rectangular waveguide and evaluated the ratio $|B_z|/|\vec{B}_t|$, which should be zero, at all element nodes. Fig. 2 shows the maximum of $|B_z|/|\vec{B}_t|$ as a function of the wavenumber. Cancellation is visible, but the peak is restricted to an extremely narrow neighborhood of the cut-off wavenumber. For practical applications, we therefore consider the axial gauge as very reliable.

Regarding the shift-and-invert preconditioner (34), plugging $k_0 = 0$ into (23) reveals that, in contrast to Section VII, only the matrix $A$ becomes singular in the static limit. Hence any non-zero shift $\bar{\lambda}$ will render the matrix $(A - \bar{\lambda}B)$ regular and hence avoid the break-down of the shift-and-invert preconditioner encountered with the $V$-gauge of Section VII.

## IX. $\psi$ Gauge

In view of (18) and (19), setting $\psi \equiv 0$ appears optimum because then neither $k_0 = 0$ nor $\gamma = 0$ can impose constraints on $\alpha$ or $\beta$, and we may formulate in $\alpha$ and $\beta$ directly. Also, the eigenvalues associated with non-physical solutions are shifted to infinity. However, unlike with the axial gauge, the algebraic eigenvalue problem (23) remains quadratic. In view of the very positive outcome of Section VIII, we believe that the solution of the quadratic problem is too expensive to compete with the axial gauge.

The variable transformation $\alpha =: \gamma\alpha'$ leads to the linearized system

$$\left( \begin{bmatrix} S_{AA}^{\nu} - k_0^2 T_{AA}^{\varepsilon} & -k_0 C_{AV}^{\varepsilon} & 0 \\ -k_0 C_{AV}^{\varepsilon T} & -S_{VV}^{\varepsilon} & 0 \\ 0 & 0 & 0 \end{bmatrix}

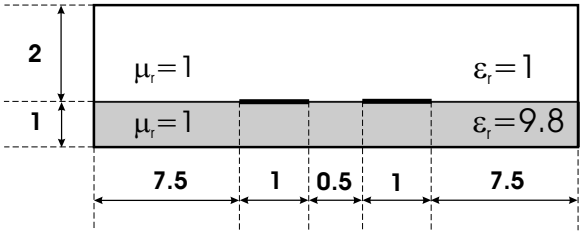


Fig. 3. Geometry of shielded microstrip transmission line. All dimensions are in mm.

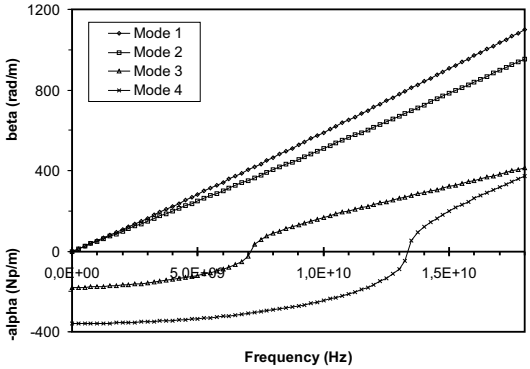


Fig. 4. Shielded microstrip: propagation characteristics of lowest order modes.

$$-\gamma^2 \begin{bmatrix} T_{AA}^{\nu\times} & 0 & B_{AV}^{\nu\times} \\ 0 & -T_{VV}^{\varepsilon} & k_0 T_{VV}^{\varepsilon} \\ B_{AV}^{\nu\times T} & k_0 T_{VV}^{\varepsilon T} & k_0^2 T_{VV}^{\varepsilon} - S_{VV}^{\nu\times} \end{bmatrix} \begin{bmatrix} \mathbf{v}_{A_t^c} \\ \mathbf{v}_{\beta} \\ \mathbf{v}_{\alpha'} \end{bmatrix} = \begin{bmatrix} 0 \\ 0 \\ 0 \end{bmatrix}, \tag{51}$$

which supports wavenumber-independent null-fields of the type

$$\gamma = 0: \qquad \alpha' = \text{arbitrary}, \qquad \vec{A}_t^c = 0, \qquad \beta = 0. \tag{52}$$

The corresponding orthogonalization condition reads

$$\mathbf{v}_{\alpha'} = (S_{VV}^{\nu\times} - k_0^2 T_{VV}^{\varepsilon})^{-1} \left( B_{AV}^{\nu\times T} \mathbf{v}_{A_t^c} + k_0 T_{VV}^{\varepsilon T} \mathbf{v}_{\beta} \right). \tag{53}$$

The transformed formulation is very similar to the axial gauge, and we have not yet been able to identify any clear advantage over the method of Section VIII.

## X. Numerical Example

Fig. 3 shows the geometry of a shielded microstrip featuring two top conductors. The structure is considered lossless but includes inhomogeneous material characteristics and sharp metal edges, and it supports two quasi-TEM modes as well as higher order box modes.

As predicted in Section VII, the $V$ gauge or field formulation, respectively, leads to poor quality solutions in the low frequency case and, below $f = 4000$Hz, it totally fails. Regarding the axial gauge of Section VIII, the variant without orthogonalization fails to converge when we approach the cut-off wavenumber of the lowest order box mode, as predicted by the theory. With orthogonalization turned on but without the splitting (12), the method fails at low frequencies because of the $1/k_0$ term in (47). However, with orthogonalization and splitting both enabled, the formulation produces reliable solutions from 18 GHz down to DC. See Fig. 4 for results. The associated FE mesh is composed of 221 triangles, the total number of unknowns is 2061, and the shift is taken to be the square of the $TE_{10}$ propagation constant of a fictitious waveguide consisting of the bounding box assuming the highest permittivity values present. Our finite element solver uses hierarchical second order $H^1$ and the corresponding mixed order $H(curl)$ elements. In the static limit, the propagation constants for the quasi-TEM modes are in the order of $\gamma^2 \approx -10^{-8}$ rather than zero. Since the lowest order box mode yields $\gamma^2 = 32227.43$, we attribute this effect to numerical noise. Since the linearized formulation of Section IX has given almost identical results including the saturation effect in the static case, no separate data are presented.

## XI. Conclusion

A general framework for a broad class of finite element waveguide solvers has been presented. Our analysis of potential- or field-based methods shows that the use of an axial gauge together with a topological splitting of the transverse field components can overcome the limitations of existing finite element formulations. The proposed method behaves very robustly in the vicinity of cut-off wavenumbers and produces reliable solutions even down at the static limit.

## References


[1] T. Ito, "Spectral domain immitance approach for dispersion characteristics of generalized printed transmission lines," *IEEE Trans. Microwave Theory Tech.*, vol. 28, pp. 733-736, July 1980.

[2] B.M.A. Rahman and J.B. Davies, "Finite-element analysis of optical and microwave waveguide problems," *IEEE Trans. Microwave Theory Tech.*, vol. 32, pp. 20-28, Jan. 1984.

[3] N. Schulz, "Finite-difference analysis of integrated optical waveguides without spurious mode solutions," *Electron. Lett.*, vol. 22, no. 18, pp. 963-965, Aug. 1986.

[4] D. Sun, Z. Cendes, "New vector finite elements for three-dimensional magnetic fields computations," *J. Appl. Phys.*, vol. 61, no. 8, pp. 3919-3921, April 1987.

[5] A. Bossavit, "A Rationale for Edge-Elements in 3-D Fields Computations," *IEEE Trans. Magn.*, vol. 24, pp. 74-79, Jan. 1988.

[6] J.F. Lee, D.K. Sun, Z.J. Cendes, "Full-Wave Analysis of Dielectric Waveguides Using Tangential Vector Finite Elements," *IEEE Trans. Microwave Theory Tech.*, vol. 39, pp. 1262 - 1271, 1991.

[7] B.M. Dillon, A.A.P. Gibson, and J.P. Webb, "Cut-off and Phase Constants of Partially Filled Axially Magnetized, Gyromagnetic Waveguides Using Finite Elements," *IEEE Trans. Microwave Theory Tech.*, vol. 41, pp. 803 - 808, 1993.

[8] B.C. Anderson, Z.J. Cendes, "Solution of Ferrite Loaded Waveguide using Vector Finite Elements," *IEEE Trans. Magn.*, vol. 31, no. 3, pp. 1578-1581, May 1995.

[9] S.V. Polstyanko and J.F. Lee, "$H_1(curl)$ Tangential Vector Finite Element Method for Modeling Anisotropic Optical Fibers," *J. Lightwave Technol.*, vol. 13, no. 11, pp. 2290-2295, Nov. 1995.

[10] S.V. Polstyanko, R. Dyczij-Edlinger, and J.F. Lee, "Fast Frequency Sweep Technique for the Efficient Analysis of Dielectric Waveguides," *IEEE Trans. Microwave Theory Tech.*, vol. 45, no. 7, pp. 1118 - 1126, 1997.

[11] F. Bertazzi, O.A. Peverini, M. Goano, G. Ghione, R. Orta, and R. Tascone, "A Fast Reduced-Order Model for the Full-Wave FEM Analysis of Lossy Inhomogeneous Anisotropic Waveguides," *IEEE Trans. Microwave Theory Tech.*, vol. 50, no. 9, pp. 2108 - 2114, 2002.

[12] R. Albanese and R. Rubinacci, "Solution of three dimensional eddy current problems by integral and differential methods," *IEEE Trans. Magn.*, vol. 24, pp. 98 - 101, 1988.

[13] I. Bardi et al., "Nodal and Edge Element Analysis of Inhomogeneously Loaded Waveguides," *IEEE Trans. Magn.*, vol. 29, pp. 1466 - 1469, 1993.